Proceedings 10th NUMGE 2023
10th European Conference on Numerical Methods in Geotechnical Engineering
Zdravkovic L, Kontoe S, Taborda DMG, Tsiampousi A (eds)

https://doi.org/10.53243/NUMGE2023-175

The influence of soil stiffness anisotropy and permeability anisotropy on the long-term response of a tunnel

A. Ruiz López[1], A. Tsiampousi[1], J.R. Standing[1], D.M. Potts[1]

[1]*Department of Civil and Environmental Engineering, Imperial College London, London, UK*

ABSTRACT: The accurate simulation of the present-day deformations and internal forces of existing tunnels is essential when predicting the available capacity of such tunnels to sustain further loading from new construction in their vicinity. In this paper, the present-day condition of a single tunnel located in the London Clay formation is simulated with a series of plane-strain finite element analyses. The focus of the numerical investigation is to evaluate the impact of soil stiffness anisotropy and permeability anisotropy on the long-term tunnel response. To evaluate the former, a comparison between analyses adopting a nonlinear isotropic stiffness model and an extension of this model considering transverse isotropic stiffness is made. The influence of the permeability anisotropy is investigated parametrically with a series of analyses varying the permeability anisotropy ratio k_h/k_v. The numerical results demonstrate the importance of considering the two aspects of soil behaviour for the simulated tunnel response to be consistent with field observations.

Keywords: finite element analysis; tunnelling; long-term movements; anisotropy

1 INTRODUCTION

Ground movements of considerable magnitude can take place long after a tunnel has been constructed in clay soils. These are caused by soil consolidation originating from the dissipation of excess pore pressures generated during tunnel construction as well as from the new drainage condition imposed by the constructed tunnel. Long-term movements can have important effects on the tunnel's deformations and internal forces.

The long-term response of tunnels in London Clay is usually characterised by a squatting deformation (enlargement of the horizontal diameter and shortening of the vertical diameter) and an increase in the axial stresses over time. Wright (2013) reported that circularity surveys carried out in running tunnels of the London Underground (LU) network indicate that these tunnels generally exhibit an average horizontal diametric distortion of between 0.5 and 1% of the internal diameter. While part of that squatting could have occurred during assembly of the tunnel rings at the time of construction, in-tunnel measurements reveal that squatting does occur over time (Ward and Thomas, 1965; Nyren, 1998). The squatting mechanism appears to be related to vertical straining taking place on the side of the tunnel (near the springline) due to drainage into the tunnel (Nyren, 1998). Barratt et al. (1994) reported axial stress measurements on a concrete tunnel taken throughout a 19.5-year period, the axial force increased, from about 25% of the overburden load shortly after construction, to about 40% and 60% at the crown and springline, respectively. Nyren (1998) reported a similar ratio between the load at the crown and springline from measurements taken on the Jubilee Line Extension eastbound tunnel. The axial stresses determined by Ward and Chaplin (1957) from measurements on GCI tunnel linings at four different sites in London were also generally larger at the springline than near the crown.

The long-term behaviour of tunnels in London Clay has been previously investigated numerically. The analyses conducted by Wongsaroj et al. (2007) produced tunnel squatting when stiffness anisotropy was adopted while significant egging (shortening of the horizontal diameter) was obtained with isotropic stiffness. Mair (2008), however, reported analysis results where the tunnel squatted using isotropic stiffness. Greater tunnel squatting was obtained as the permeability anisotropy became larger. Shin et al. (2002) investigated numerically the long-term axial forces of a tunnel, while the forces increased over time around the tunnel (when the tunnel was impermeable), they were larger at the crown and invert than at the springline which is opposite to the trends observed in the field.

The results of a series of 2D analyses investigating the effect of soil stiffness anisotropy and permeability anisotropy on the tunnel's present-day deformations and internal forces are presented in this paper. The analyses were carried out using the Imperial College Finite Element Program ICFEP (Potts and Zdravkovic, 1999). The numerical results reveal that considering both soil stiffness anisotropy and permeability anisotropy is vital to achieve tunnel deformations and forces matching those observed in the field.

2 DESCRIPTION OF THE NUMERICAL MODEL

2.1 Geometry

The soil stratigraphy employed in the analyses is depicted in Figure 1. The stratigraphy comprised 3 m of superficial deposits (SD) overlying a total of 57 m of London Clay (LC), 6 m of Upper Lambeth Group (ULG) and 6 m of Lower Lambeth Group (LLG). A single tunnel of 3.81 m external diameter with its crown located at 20 m depth was considered. The size and properties, discussed in Section 2.2, adopted for the tunnel represented a standard GCI lining of the LU network. Symmetry conditions were applicable around the axis of the tunnel so that it was only necessary to consider half of the domain.

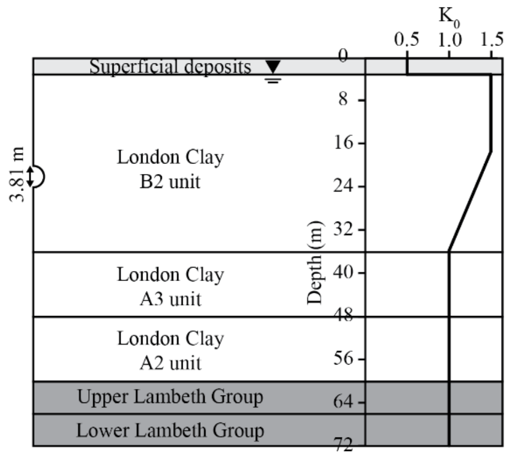

Figure 1. Stratigraphy and K_0 profile considered in the analyses

2.2 Soils and tunnel lining modelling

The mechanical behaviour of London Clay was simulated with both nonlinear isotropic stiffness and transverse isotropic stiffness along with the perfectly-plastic Mohr-Coulomb (MC) failure criterion. The IC.G3S model (Taborda et al., 2016) was used as the isotropic stiffness model while the adopted transverse isotropic stiffness model was an extension of the IC.G3S incorporating the three-parameter formulation for transverse isotropy of Graham and Houlsby (1983). The transverse isotropic model was first employed by Zdravkovic et al. (2021) for the simulation of laterally-loaded monopiles in London Clay.

It was assumed that the three London Clay subdivisions shown in Figure 1 had the same mechanical response and the same model parameters were adopted for them. These were calibrated against the laboratory and field investigation conducted in the Heathrow Airport Terminal 5 site (Gasparre, 2005; Gasparre et al., 2007; Hight et al., 2007). The transverse isotropic stiffness model requires the shear modulus in the vertical plane G_{vh}, the Poisson's ratio for the horizontal strains due to horizontal strains μ_{hh} and the stiffness anisotropy ratio α as input parameters and determines the remaining components of the stiffness matrix using Graham and Houlsby's (1983) formulae. *Table 1* presents the values adopted for the parameters controlling the degradation of G_{vh} with strain. The stiffness anisotropy ratio at small strains α_{ss} was taken as 2, this value was decided based on the ratio between the shear moduli in the vertical and horizontal planes G_{vh}/G_{hh} established from laboratory and field measurements. It was assumed that the anisotropy ratio α reduced upon shearing from α_{ss} to α_{ls}=1, its value at large strains. a_α and b_α, the parameters controlling the variation of α with strain, were adopted as 0.002 and 2, respectively (Ruiz López, 2022). These two parameters were adjusted for the model to provide a good match with the five undrained triaxial compression (TXC) stress paths shown in Figure 2, i.e., the inclination of the stress paths depends on the stiffness anisotropy ratio α. The Poisson's ratio μ_{hh} adopted a constant value of 0.1 that was determined based on the laboratory measurements of Gasparre et al. (2007). The parameters defining the shear stiffness and bulk stiffness degradation of the (isotropic) IC.3GS model are given in *Table 2* and *Table 3*, respectively. Note that the shear stiffness degradation for the IC.3GS model is analogous to that defined for G_{vh} in the transverse isotropic model. As shown in Figure 2, the stress paths for undrained TXC obtained with the IC.3GS model are vertical. The vertical stress path is explained by the lack of coupling between volumetric and deviatoric components of the stress-strain relationship when adopting isotropic stiffness. The parameters of the MC failure criterion are presented in *Table 4*.

Table 1. Parameters defining the nonlinear degradation of shear stiffness Gvh (p'ref =1.0 kPa; mG=1.0)

Material	$G_{0,vh}$ (kPa)	a	b	$R_{G,min}$	$G_{min,vh}$ (kPa)
LC	200.0	$5.0\cdot10^{-4}$	1.50	0.140	2667

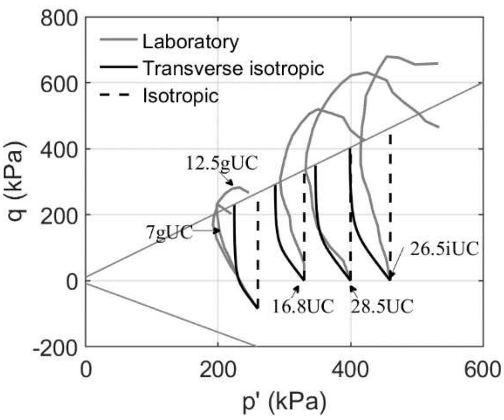

Figure 2. Simulated undrained triaxial compression tests along with laboratory data from Gasparre (2005)

The superficial deposits were simulated as linear elastic along with the MC failure criterion. An elastic modulus of 10 MPa and a Poisson's ratio of 0.2 were adopted. The two Lambeth Group layers were modelled with the IC.3GS model along with the MC failure criterion. The adopted parameters defining the nonlinear degradation of the shear stiffness and bulk modulus are presented in *Table 2* and *Table 3*, respectively. The corresponding parameters of the MC criterion for the superficial deposits and Lambeth Group layers are given in *Table 4*.

The tunnel lining was simulated with beam elements and as a linear elastic material. An elastic modulus of 100 GPa and a Poisson's ratio of 0.26 were employed, both of which are representative of the elastic behaviour of GCI. The adopted cross-section area and second moment of area were $3.61 \cdot 10^{-2}$ m^2/m and $4.58 \cdot 10^{-5}$ m^4/m.

Table 2. Parameters defining the nonlinear degradation of isotropic shear stiffness G (p'ref =1.0 kPa; mG=1.0)

Material	G_0 **(kPa)**	a	b	$R_{G,min}$	G_{min} **(kPa)**
LC	200.0	$5.0 \cdot 10^{-4}$	1.50	0.140	2667
ULG	334.5	$1.1 \cdot 10^{-4}$	1.20	0.067	2000
LLG	377.0	$9.5 \cdot 10^{-5}$	1.04	0.090	2000

Table 3. Parameters defining the nonlinear degradation of isotropic bulk stiffness K (p'ref =1.0 kPa; mG=1.0)

Material	K_0 **(kPa)**	r	s	$R_{K,min}$	K_{min} **(kPa)**
LC	200.0	$1.2 \cdot 10^{-4}$	2.31	0.135	2500
ULG	300.0	$6.5 \cdot 10^{-5}$	1.10	0.096	2500
LLG	449.7	$2.4 \cdot 10^{-4}$	1.10	0.085	2500

Table 4. Mohr-Coulomb parameters and unit weights

Material	c' **(kPa)**	φ' (°)	ψ (°)	γ **(kN/m³)**
SD	0.0	25.0	0.0	18.0
LC	5.0	25.0	0.0	20.0
ULG	10.0	28.0	0.0	20.0
LLG	0.0	36.0	18.0	20.0

2.3 Initial conditions and permeability profile

The profile of the coefficient of earth pressure at rest K_0 with depth is shown in Figure 1 along with the soil stratigraphy. The value of K_0 reduced linearly from 1.5 at a depth of 17.4 m to 1 at the top of the A3 unit, at 36 m depth. An initial hydrostatic pore pressure profile was adopted with the water table set at 3 m depth.

The permeability profile adopted in the analyses is one of the factors governing the response of the soil-tunnel system. Figure 3 presents field measurements of horizontal permeability k_h values from several sites across London collected by Hight et al. (2007) along with the stratigraphy of the analyses. While it seems clear that, in London Clay, the horizontal permeability k_h is larger than the vertical permeability k_v (Chandler et al., 1990), the actual magnitude of the permeability anisotropy ratios k_h/k_v is less obvious. Previous numerical investigations on tunnelling-induced long-term movements in London Clay have adopted a range of k_h/k_v. ratios: Mair (2008) employed a ratio of 4, Wongsaroj et al. (2013) adopted ratios of 2 and 10 and Avgerinos et al. (2016) used k_h/k_v=2 for the whole stratigraphy except for the top of the London Clay A3 unit where they adopted ratios of 2, 25 and 100. None of these studies, however, evaluated systematically the effect of k_h/k_v on a tunnel long-term structural response. The analyses of this investigation adopted an anisotropic permeability model that allows permeability to vary logarithmically with depth according to the following expression:

$$k = k_0 \cdot 10^{G_z (z - z_0)} \qquad (1)$$

where k_0 is the permeability value at the reference depth z_0, z is the depth and G_z is the parameter controlling the variation of permeability with depth. The ratio k_h/k_v was varied while keeping constant the profile of $k_{soil}=\sqrt{k_h\, k_v}$ such that the profiles of k_h and k_v both varied along with k_h/k_v. A permeability anisotropy ratio k_h/k_v equal to 8 was adopted when evaluating the effect of soil stiffness anisotropy; when investigating the influence of the k_h/k_v ratio, values of 1, 2, 4, 8 and 16 were considered. The reference depth z_0 in Expression 1 was set to 3 m (top of London Clay), the reference permeability k_0 was equal to $14.1 \cdot 10^{-10}$ m/s and G_z was set to 0.025 m^{-1}. The profiles of k_h and k_v used in the analyses were defined adjusting the value of k_0 according to the corresponding k_h/k_v ratio. The profile for permeability k_{soil} is shown in Figure 3 along with the profiles of k_h and k_v for k_h/k_v=16. Even for the latter ratio, the largest considered, the permeability profiles plot well within the range of field measurements.

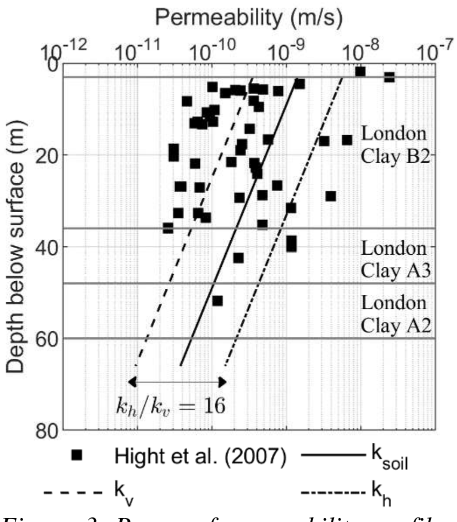

Figure 3. Range of permeability profiles with depth along with the field data reported by Hight et al. (2007)

2.4 Boundary conditions

Regarding the mechanical boundary conditions, the horizontal displacements of the two vertical boundaries were restrained; the vertical and horizontal displacements of the bottom boundary were also restrained. Additionally, rotations of the tunnel lining nodes at the plane of symmetry were fixed.

With respect to the hydraulic boundary conditions, the superficial deposits and Lower Lambeth Group were assumed to be drained and so a condition of zero pore pressure change was prescribed on their respective interfaces with the London Clay and Upper Lambeth Group layers. A zero pore pressure change was also prescribed on the far-field vertical boundary while a non-flow condition was applied to the vertical symmetry boundary. The precipitation boundary condition (Potts and Zdravkovic, 1999), was applied to the tunnel boundary. It was utilised in a way such that if the pore pressure magnitude at a given node was compressive at the start of an increment, the algorithm assigned a zero pore pressure to that node; conversely, if the pore pressure was tensile (suction) a zero flow boundary was assigned.

2.5 *Analysis details*

The excavation of the tunnel was conducted by incrementally reducing the nodal forces, corresponding to the initial total stresses, acting around the tunnel boundary while gradually ramping up an isotropic radial pressure such that only this pressure was active by the end of the excavation. The construction sequence was completed by activating the tunnel lining and subsequently releasing the radial pressure. The magnitude of the latter was adjusted through trial and error to match a volume loss of approximately 1.5% at the end of tunnel construction.

Coupled consolidation was simulated throughout the analyses. The period of tunnel excavation and construction was defined as 36 hours (López et al., 2021). After tunnel construction, a consolidation period of 130 years was considered, representing the time span from the construction of the oldest GCI tunnels to the present day.

3 INFLUENCE OF SOIL STIFFNESS ANISOTROPY

The influence of soil stiffness anisotropy on the pore pressure response around the tunnel is considered first. Figure 4 presents the pore pressure profiles, above the tunnel and with distance from the tunnel springline, immediately after construction and at the present day. While the pore pressure distribution in the long term only depends on the hydraulic boundary conditions and permeability values and is therefore unaffected by the adopted constitutive model, the effect of the stiffness anisotropy is apparent immediately after construction. Above the tunnel crown, the pore pressures after construction reduce below the initial hydrostatic profile when the transverse isotropic model is adopted while they are slightly larger from about 1 m above the tunnel crown when the isotropic stiffness model is used. The opposite trend is observed on the side of the tunnel: with the transverse isotropic model, there is an increase in the pore pressures, with respect to the hydrostatic value from about 3.5 m to 20 m from the springline; with the isotropic model, the pore pressures fall below the hydrostatic value along the first 10 m from the springline. The pore pressure response obtained with the isotropic model is entirely explained by the changes in the total mean stress which are compressive above the tunnel and tensile on the side of the tunnel. Conversely, pore pressure changes are also induced by shearing when the transverse isotropic model is employed; in particular, the soil adjacent to the springline is subjected to stress conditions similar to undrained triaxial compression which generate positive excess pore pressures (as inferred from Figure 2) while the stress conditions above the tunnel are akin to undrained triaxial extension which lead to negative excess pore pressures.

In relation to the tunnel response, Figure 5 presents the change in radius (in % of the tunnel radius) and the axial forces (kN) around the tunnel at present day. Note that the forces given by the plane-strain analysis, in kN/m units, were multiplied by the width of a tunnel ring (≈0.5 m). The tunnel deforms into the squatting mode in the two analyses which is due to the greater consolidation taking place on the side of the tunnel than above (and below) the tunnel, implied in Figure 4. This trend is more exacerbated in the analysis adopting the transverse isotropic model which gives a tunnel squat of 0.51% whereas a tunnel squat of 0.21% is obtained with the isotropic model. While the former magnitude falls at the lower end of the range of squatting magnitudes expected in the field (0.5-1%) that corresponding to the isotropic model is significantly lower than the expected values. The reduction of the vertical diameter is approximately of the same magnitude as the increase of the horizontal diameter in both cases. The bending mode experienced by the tunnel largely explains the axial forces at the springline being larger than those at the crown and invert in both analyses. Because the tunnel lining is subjected to less bending when the isotropic model is employed, it sustains a smaller variation in axial forces around the ring than in the analysis using the transverse isotropic model.

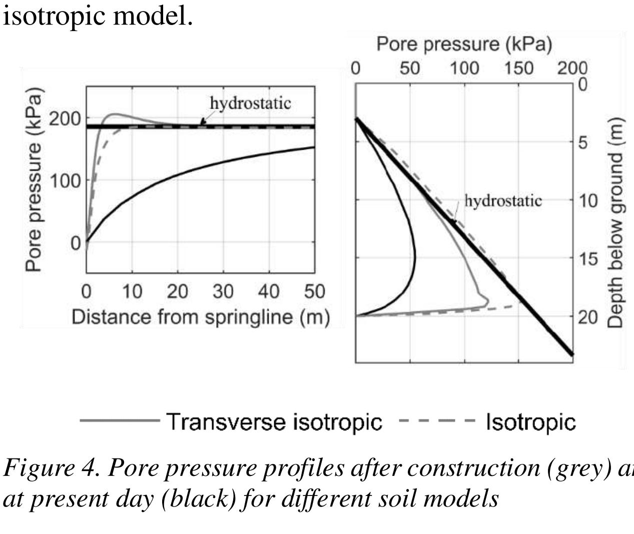

Figure 4. Pore pressure profiles after construction (grey) and at present day (black) for different soil models

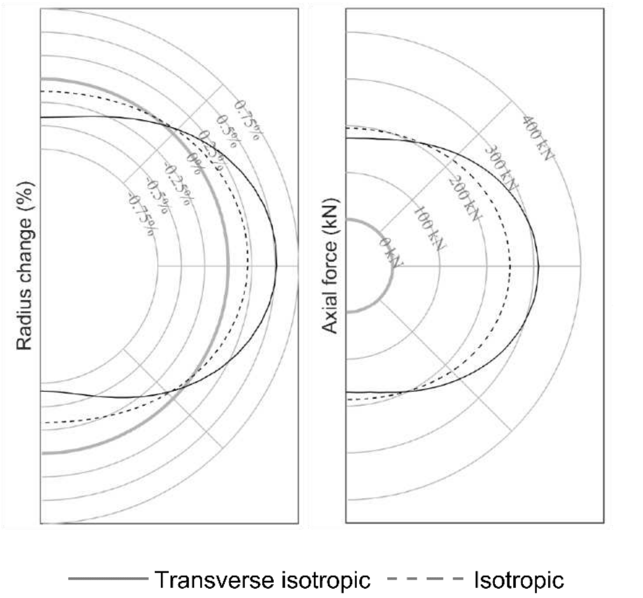

Figure 5. Deformations and axial force around the tunnel at present day for different soil models

4 INFLUENCE OF PERMEABILITY ANISOTROPY RATIO

The pore pressure profiles after construction and at the present day with distance from the springline and above the tunnel crown obtained with different k_h/k_v ratios are shown in Figure 6. Only small differences can be observed between the pore pressure profiles after construction obtained with different k_h/k_v ratios, however, the effect of k_h/k_v on the long-term pore pressure is evident. Above the tunnel crown, smaller k_h/k_v ratios produced lower pore pressures whereas the opposite trend is observed on the side of the tunnel. While greater consolidation takes place near the springline than above the tunnel for all cases, larger differences between the two locations are obtained with larger k_h/k_v ratios.

The tunnel deformations and forces at the present day are shown in Figure 7. It can be observed that larger k_h/k_v ratios yield greater tunnel deformations. Due to the larger consolidation occurring on the side of the tunnel, with respect to above the crown (and below the invert) all analysis cases produce squatting of the tunnel. The tunnel squatting varies between 0.27% for the isotropic permeability case (k_h/k_v=1) and 0.56% for k_h/k_v=16 and lies within the typical values measured in the field (0.5-1% as reported by Wright, 2013) for k_h/k_v ratios equal or greater than 8. The influence of k_h/k_v is not linear as increasingly smaller differences in tunnel squat as well as vertical distortion are found for larger k_h/k_v ratios. Consistent with the bending mode experienced by the tunnel lining, greater k_h/k_v ratios increase the axial forces at the springline and reduce them at the crown and invert. The k_h/k_v ratio affects significantly more the axial forces at the springline than at the crown because, as noted by Ruiz López (2022), the axial loading developed by the crown and invert cross-sections is predominantly governed by the drainage condition adopted for the lining (less permeable linings attracting greater loads) which is the same for all analyses while the axial compression at the springline is mostly controlled by bending (greater squatting associated to larger forces). Lastly, the distribution of axial forces qualitatively agrees with the field measurements taken by Ward and Chaplin (1957) which generally indicated larger axial stresses at the springline than around the crown.

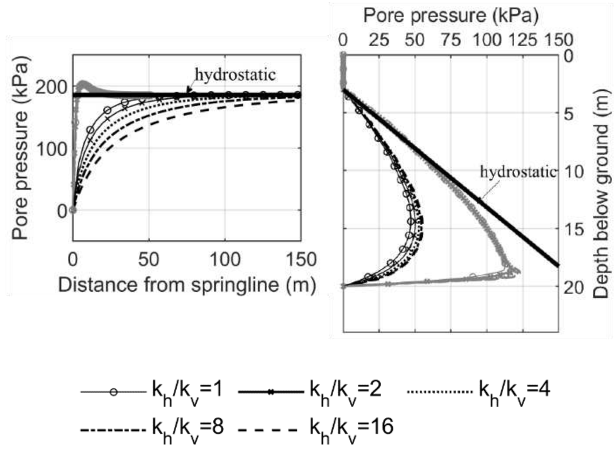

Figure 6. Pore pressure profiles after construction (grey) and at present day (black) for different k_h/k_v ratios

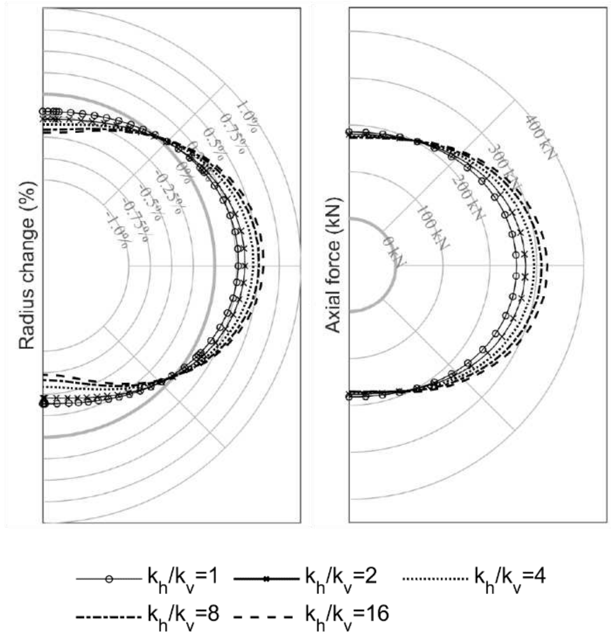

Figure 7. Deformations and axial force around the tunnel at present day for different k_h/k_v ratios

5 CONCLUSIONS

A numerical parametric study investigating the effect of soil stiffness anisotropy and the permeability anisotropy ratio on a tunnel's present-day deformations and internal forces is described in this paper. Considering soil stiffness anisotropy affected considerably the pore pressure distribution after construction of the tunnel which led to tunnel squatting within the range expected for a tunnel of the LU network while the analysis adopting isotropic stiffness produced significantly less squatting. The permeability anisotropy ratio k_h/k_v also had a significant influence on the tunnel response. Increasing levels of permeability anisotropy produced greater and lesser consolidation on the side of the tunnel and above/below the tunnel, respectively, with an associated increase in squatting and bending of the tunnel. This study demonstrates that considering both soil stiffness anisotropy and permeability anisotropy is required to achieve realistic numerical predictions of the present-day condition of tunnels in London Clay.

6 ACKNOWLEDGEMENTS

This research was funded by the Engineering and Physical Sciences Research Council (EPSRC) through a Doctoral Training Grant (EP/R512540/1) awarded to the first author.

7 REFERENCES

Avgerinos, V., Potts, D., Standing, J. (2016). The use of kinematic hardening models for predicting tunnelling-induced ground movements in London Clay. *Géotechnique*, 66(2), 106–120.

Barratt, D., O'Reilly, M., Temporal, J. (1994). Long-term measurements of loads on tunnel linings in overconsolidated clay. In *Tunnelling'94* (pp. 469–481). Springer.

Chandler, R. J., Leroueil, S., Trenter, N. A. (1990). Measurements of the permeability of London Clay using a self-boring permeameter. *Géotechnique*, *40*(1), 113-124.

Gasparre, A. (2005). *Advanced Laboratory Characterization of London Clay*. PhD thesis, Imperial College London (University of London).

Gasparre, A., Nishimura, S., Minh, N., Coop, M., Jardine, R. (2007). The stiffness of natural London Clay. *Géotechnique*, 57(1), 33–47.

Graham, J., Houlsby, G. (1983). Anisotropic elasticity of a natural clay. *Géotechnique*, 33(2), 165–180.

Hight, D., Gasparre, A., Nishimura, S., Minh, N., Jardine, R., Coop, M. (2007). Characteristics of the London Clay from the Terminal 5 site at Heathrow Airport. *Géotechnique*, 57(1), 3–18.

López, A. R., Tsiampousi, A., Taborda, D. M. G., Standing, J. R., Potts, D. M. (2021). Numerical investigation into time-dependent effects on short-term tunnelling-induced ground response in London Clay. In *Geotechnical Aspects of Underground Construction in Soft Ground*, 597-604. CRC Press.

Mair, R. J. (2008). Tunnelling and geotechnics: new horizons. *Géotechnique*, 58(9), 695–736.

Nyren, R. (1998). *Field measurements above twin tunnels in London Clay*. PhD thesis, Imperial College, University of London.

Potts, D. M., Zdravkovic, L. 1999. *Finite element analysis in geotechnical engineering: theory*, Thomas Telford, London.

Ruiz López, A. D. (2022) *Development of advanced numerical models for grey cast iron tunnel linings*. PhD Thesis, Imperial College London.

Shin, J., Addenbrooke, T., Potts, D. (2002). A numerical study of the effect of groundwater movement on long-term tunnel behaviour. *Géotechnique*, 52(6), 391–403.

Taborda, D., Potts, D. M., Zdravkovic, L. (2016). On the assessment of energy dissipated 918 through hysteresis in finite element analysis. *Computers and Geotechnics*, 71, 180–194.

Ward, W., Chaplin, T. (1957). Existing stresses in several old London Underground tunnels. In *Proc 4th Int Conf Soil Mech and Found Engrg, London*, volume 2 (pp. 256–259).

Ward, W., Thomas, H. (1965). The development of earth loading and deformation in tunnel linings in London Clay. In *Proceedings of the Sixth International Conference on Soil Mechanics and Foundation Engineering, 1965*, volume 2 (pp. 432–436).

Wongsaroj, J., Soga, K., Mair, R. (2007). Modelling of long-term ground response to tunnelling under St James's Park, London. *Géotechnique*, 57(1), 75–90.

Wongsaroj, J., Soga, K., Mair, R. (2013). Tunnelling-induced consolidation settlements in London Clay. *Géotechnique*, 63(13), 1103–1115.

Wright, P. J. (2013). Validation of soil parameters for deep tube tunnel assessment. *Proceedings of the Institution of Civil Engineers-Geotechnical Engineering*, 166(1), 18–30.

Zdravković, L., Potts, D. M., Taborda, D. M. (2021). Integrating laboratory and field testing into advanced geotechnical design. *Geomechanics for Energy and the Environment*, *27*, 100216.